Jordanian Journal of Computers and Information Technology (JJCIT), Vol. 09, No. 04, December 2023.

DESIGN OF MICROSTRIP DUAL-BAND BANDPASS FILTER FOR SUB-6 GHZ 5G MOBILE COMMUNICATIONS

Rachida Boufouss and Abdellah Najid

(Received: 7-Jul.-2023, Revised: 12-Aug.-2023, Accepted: 2-Sep.-2023)

ABSTRACT

In this paper, a microstrip bandpass filter for dual-band sub-6 GHz 5G mobile communications is designed. The two first resonance frequencies of the stepped-impedance resonator are used as the operating frequencies of the two passbands. Furthermore, the stepped-impedance resonator is folded to form an open-loop stepped-impedance resonator for compactness. This form of the resonator generates a second transmission zero in the upper stopband, which improves the out-of-band rejection. A 50 Ω *tapped-line input/output is used to feed the filter. The proposed structure is designed, analyzed and manufactured and the measured results are found to be in good agreement with the simulation results. From the measured results, it is found that the proposed filter achieved a return loss of 21.5 dB and 28.3 dB, an insertion loss of 0.4 dB and 1.7 dB and a bandwidth of 12.5% and 10.81% at 3.61 GHz and 5.55 GHz, respectively. In addition, the proposed filter has a compact size, which makes it suitable for sub-6 GHz 5G mobile communications.*

KEYWORDS

5G, Bandpass filter, Dual-band, Stepped-impedance resonators, Sub-6 GHz.

1. INTRODUCTION

The growing demand for mobile-phone users, connected devices and the proliferation of applications requiring high data rates have led to jump to the fifth generation (5G). Compared with 4G, the 5G will enable to deliver higher data rates: 1000 times faster than 4G [1]. Many countries have started to deploy 5G networks and have awarded it frequency bands. In sub-6 GHz spectrum, the 3.6 GHz band (3400-3800 MHz) is allocated by many countries for 5G mobile communications, such as the European Union and the United Kingdom [2]. Besides that, the unlicensed band (5150-5925 MHz) has also been added to the 5G spectrum to support the existing licensed 5G bands. Therefore, designing microwave components, such as bandpass filters (BPFs) with compact size and good electrical performance operating in these two bands, is necessary to meet the requirements of 5G.

In literature, numerous technologies have been used to design BPFs for sub- 6 GHz applications [3]-[13]. Among these, dual-band BPFs using substrate-integrated waveguides (SIWs) are reported in [3] and [4], the size of the filter in [3] is relatively large, while the filter in [4] provides a low return loss. A CPW BPF based on spiral-shaped DGSs is designed to operate at 3.54 GHz in [5] and its 3-dB bandwidth is ranging from 3.29 GHz to 3.79 GHz with an insertion loss less than 2 dB over the passband. In [6], a dual-band BPF consisted of folded open-circuited stubs with interdigital unit cells is proposed, but its circuit size is large. In [7], a dual-band BPF is designed using substrate-integrated suspended line (SISL) technology to operate at 3.45/4.9 GHz. The two passbands are formed by using quarter-wavelength stepped-impedance resonators (QSIRs) and half-wavelength hairpin resonators (HWHRs). In [8], a dual-band BPF using a dual-mode dielectric waveguide resonator operates at 2.1/3.53 GHz with a fractional bandwidth of 2.27/1.67% is reported. A dual-band BPF with interlocked stepped-impedance resonators operating at 0.946/1.48 GHz (SIRs) is presented in [9]. The filter has a compact size, but the insertion loss is relatively high. A wideband bandpass spatial filter using a double square loop frequency-selective surface (DSLFSS) is proposed in [10]. However, all these reported BPFs will work only for the 5G licensed bands and to the authors' knowledge, there is no dual-band BPF that covers both the licensed and unlicensed 5G bands in the literature.

In this paper, a low-cost microstrip dual-band BPF using two stepped-impedance resonators (SIRs) for 5G mobile communications is designed to cover the licensed 5G band 3600-3800 MHz and the unlicensed

R. Boufouss and A. Najid are with Department of Communication Systems, National Institute of Posts and Telecommunications, Rabat, Morocco.
Emails: boufouss.rachida@gmail.com and najid@inpt.ac.ma

5G band 5150-5925 MHz. The two first resonant mode frequencies of the SIR are used as the center frequencies of the first and second passbands of the filter. In addition, to further reduce the size of the circuit, SIRs are folded to form open-loop SIRs. By choosing the appropriate value of the gap between the edges of the high-impedance lines, a second transmission zero is generated in the upper stopband, which helps to improve the rejection level of the filter. The proposed dual-band BPF is designed, simulated and manufactured. The results of simulation and those of experiment are in good agreement. Moreover, the experiment results are compared with existing 5G filters.

The organization of the paper is as follows: In Section 2, resonance properties of the SIR and open-loop SIR are discussed based on the even-odd mode analysis and the design procedure of the proposed dual-band BPF is presented. The experimental validation is shown in Section 3. Finally, conclusions drawn are given in Section 4.

2. MICROSTRIP DESIGN OF DUAL-BAND BPF

2.1 Analysis of the Typical SIR and Open-Loop SIR

In principle, the typical λ/2 SIR is composed of a λ/4 low-impedance line (Z_1, $2\theta_1$) and two-high λ/8 impedance lines at both ends (Z_2, θ_2), as depicted in Figure 1. Given that the structure is symmetrical, even- and odd-mode analysis can be utilized to describe the resonator. The even- and odd-mode equivalent circuits of the typical SIR are shown in the same figure. For simplicity, we choose $\theta = \theta_1 = \theta_2$.

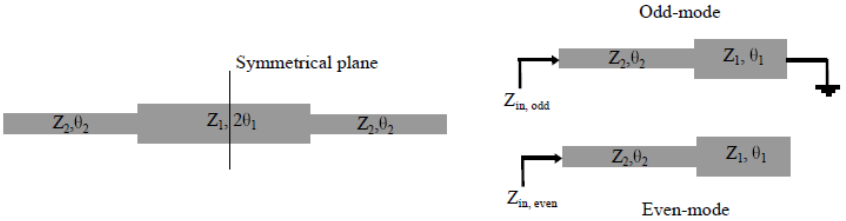

Figure 1. Structure of the traditional SIR with even- and odd-mode equivalent circuits.

The input impedance can be expressed for the odd mode [13] as:

$$Z_{in,odd} = jZ_2 \frac{\tan\theta + R_Z \tan\theta}{R_Z - tan^2\theta} \quad (1)$$

where R_Z is the ratio between the high- and low-impedance lines. By imposing zero input admittance of the odd mode ($Y_{in,odd} = 1/Z_{in,odd}$), the first and the third resonant mode frequencies of the SIR can be written as:

$$\theta(f_1) = tan^{-1}\sqrt{R_Z} \quad (2)$$

$$\theta(f_3) = \pi - tan^{-1}\sqrt{R_Z} \quad (3)$$

Similarly, for the even mode, the input impedance can be derived as [13]:

$$Z_{in,even} = jZ_2 \frac{R_Z tan^2\theta - 1}{tan\theta(R_Z + 1)} \quad (4)$$

The second and the fourth even-mode resonance frequencies can be deduced from Equation (4) by imposing zero input admittance of the even mode:

$$\theta(f_2) = \frac{\pi}{2} \quad (5)$$

$$\theta(f_4) = \pi \quad (6)$$

For miniaturization, the typical SIR shown in Figure 1 is folded to form an open-loop SIR, as depicted in Figure 2 with its even- and odd-mode equivalent circuits. Here, C models the electric coupling capacitance between the edges of the high-impedance lines. With the presence of this capacitance on the odd-mode equivalent circuit, the total electrical lengths at the odd-mode resonance frequencies increase, while in the even mode, these lengths are kept constant (the even-mode equivalent circuit for the open-loop SIR is the same as that of the typical SIR). Therefore, the resonance frequencies of the open-loop SIR f_1 and f_3 shift down to the lower frequencies.

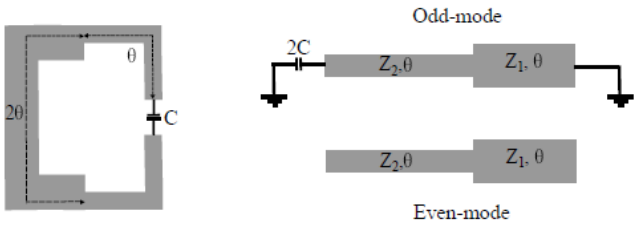

Figure 2. Structure of the open-loop SIR with even- and odd-mode equivalent circuits.

2.2 BPF Design

Figure 3 depicts the proposed structure of the dual-band BPF using two open-loop SIRs with 50 Ω tapped line input/output on an RT/Duroid 5870 substrate of 0.79-mm thickness and with a dielectric constant of 2.33 and a loss tangent of 0.0012. As a first step, the center frequencies of the first and second passbands f_1 and f_2 of the filter are taken as 3.5 GHz and 5.5 GHz, respectively. The calculated impedance ratio Rz is 2.75 and the initial SIR dimensions are determined using the above equations. Then, the two SIRs are folded and used to design the dual-band BPF. A full-wave EM simulator (CST Microwave Studio) is used to simulate the filter. As expected, a deviation between the analytical and simulation results has been found. This deviation is caused by the coupling between the edges of the high-impedance line sections, C, mentioned above and the coupling between resonators since in the analysis one SIR has been considered.

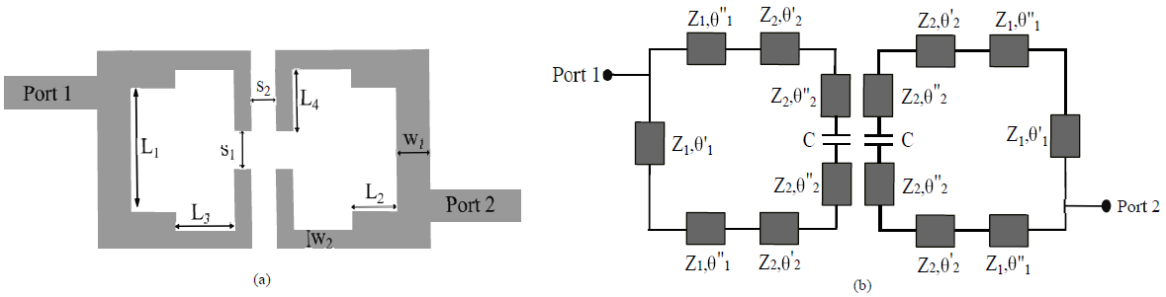

Figure 3. (a) Structure of the proposed dual-band BPF. (b) Its equivalent circuit model ($\theta = \frac{\theta_1'}{2} + \theta_1'' = \theta_2' + \theta_2''$).

To visualize the change of the magnitude S_{21} of the filter with different couplings, two simulations are displayed in Figure 4. It can be seen from the left part of the figure that, for a specific value of the gap between the edges of the high-impedance lines and besides the existing transmission zeros in the upper stopband, another transmission zero starts to appear and shifts to the upper frequencies when S_1 increases. In addition to that, the rejection level is enhanced in the upper stopband when the two transmission zeros are closer to each other.

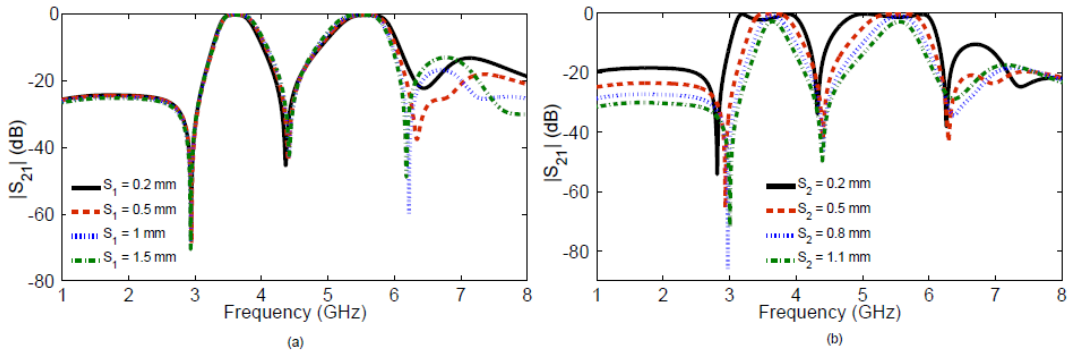

Figure 4. Variation of magnitude of insertion loss S_{21} (a) *Versus* S_1. (b) *Versus* S_2.

From the right part of the figure, it is clearly observed that the separation between resonators determines the bandwidth of the filter. As S_2 decreases, the bandwidth of the filter increases and the rejection level in the lower and upper stopband decreases. It should be noted that the bandwidth of the filter is also controlled by the external quality factor of the filter which is determined by the position of the tapped

input and output lines. Therefore, by choosing the appropriate position of the tapped lines and adjusting the separation between resonators, the desired bandwidth can be achieved.

After optimization, the dimensions of the BPF are determined, as listed in Table 1. The simulation results are shown in Figure 5. It is seen that the working bands of the proposed dual-band BPF are 3380-3870 MHz and 5149-5840 MHz with insertion losses of 0.37 dB and 0.42 dB and return losses of 26.2 dB and 31.1 dB at 3.6 GHz and 5.55 GHz, respectively. Four transmission zeros are found at f_{z1} = 2.93 GHz, f_{z2}= 4.39 GHz, f_{z3} = 6.29 GHz and f_{z4} = 6.86 GHz. The rejection level in the upper stopband is about 19.4 dB.

Table 1. Dimensions of the proposed filter.

Parameter	**Value**	**Parameter**	**Value**
W_1	2.37	L_3	3.17
W_2	0.24	L_4	6.9
L_1	10.11	S_1	0.57
L_2	2.9	S_2	0.58

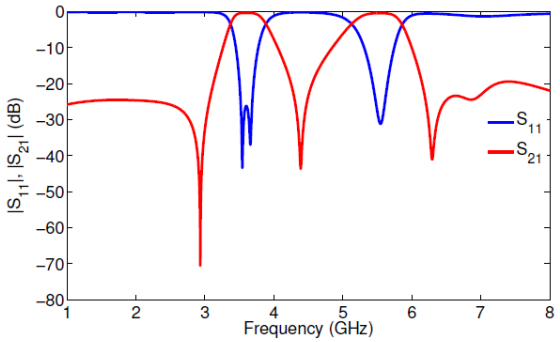

Figure 5. Simulation results of the proposed filter.

The current distributions of the proposed BPF are displayed in Figure 6. It is clearly observed that no current flows through port 1 to port 2 at the frequencies of the transmission zeros, while the current passes between the two ports at the center frequencies of the BPF, which indicates the BPF behavior of the structure.

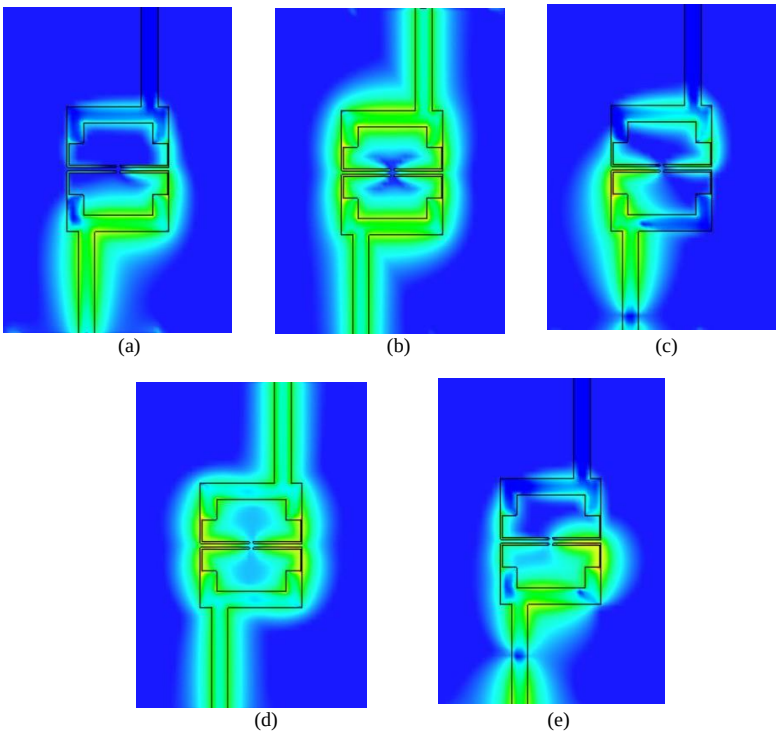

Figure 6. Simulated current distribution of the proposed dual-band BPF: (a) at 2.93 GHz. (b) at 3.6 GHz. (c) at 4.39 GHz. (d) at 5.5 GHz and (e) at 6.29 GHz.

3. IMPLEMENTATION AND RESULTS

The filter designed above has been fabricated on the same substrate and measured using VNA Master MS 2028C. Its fabricated prototype and measurement equipment are presented in Figure 7. Figure 8 depicts both simulation and experimental results of the proposed filter. Good agreement between them have been observed. It can be seen that the realized dual-band BPF operates at 3.61 GHz and 5.55 GHz with a 3-dB fractional bandwidth of 12.5% and 10.81%. Measured insertion losses at 3.61 GHz and 5.55 GHz center frequencies are 0.4 dB and 1.7 dB, corresponding to 21.5 dB and 28.3 dB return losses, respectively. The lower stopband rejection is better than 23.8 dB from 1 to 3.1 GHz, while in the upper stopband, it is 19.8 dB. Four measured transmission zeros located at f_{z_1} = 2.94 GHz, f_{z_2} = 4.46 GHz, f_{z_3} = 6.36 GHz and f_{z_4} = 6.82 GHz. The occupied size of this filter without feed lines is $0.25\lambda_g \times 0.30\lambda_g$, where λ_g is the guided wavelength at 3.61 GHz.

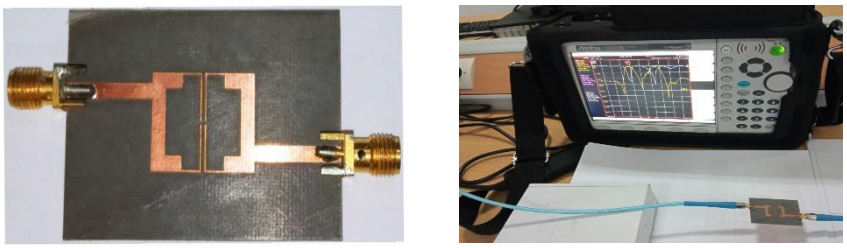

(a) (b)

Figure 7. (a) Photograph of the fabricated dual-band BPF. (b) Its measurement equipment.

The group delay of the proposed dual-band BPF is displayed in Figure 9. It can be seen that the filter has a flat response within the passbands. The group delay is below 1.5 ns in the first passband, while it is below 1.2 ns in the second passband.

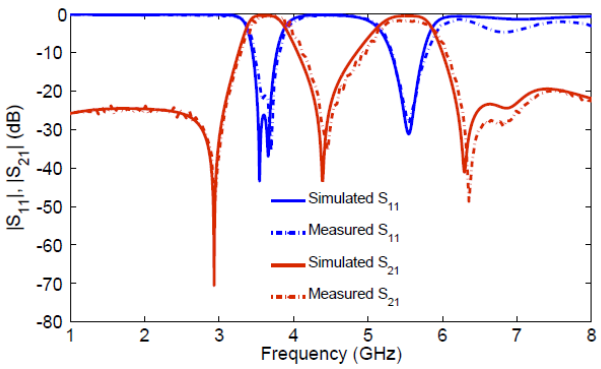

Figure 8. Simulated and measured S-parameters of the dual-band BPF.

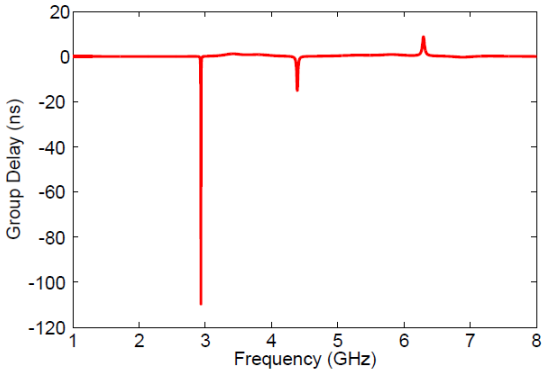

Figure 9. Group delay of the dual-band BPF.

Table 2. Comparison between this work and other previous 5G BPFs.

Ref.	CFs (GHz)	FBW (%)	IL (dB)	RL (dB)	Out-of-band rejection (dB)	Size ($\lambda_g \times \lambda_g$)
[3]	3.5/4.9	-	0.75/1.3	-	-	1.61×1.23
[4].A	2.66/3.54	7.89/4.52	0.86/1.53	>18/>15.4	> 20 (3.8–4.2 GHz)	0.122×0.22
[4].B	2.82/3.73	6.38/3.84	0.76/1.93	>13.5/>20	16 (3.88–5 GHz)	0.34×0.24
[4].C	2.84/3.74	5.98/3.47	1.72/2.02	>12.4/>17	16 (3.88–5)	0.34×0.24
[5]	3.54	10.1	1.23	28.9	>20 (4.29-7 GHz)	0.42×0.37
[7]	3.45/4.9	11/6.9	0.85/1.13	–	–	0.32×0.45
[8]	2.91/3.53	2.27/1.67	1/1.5	17/18	>28	-
[9]	0.946/1.48	9.8/9.5	2.16/1.26	>10/>10	11.37 (1.6–2 GHz)	0.25×0.12
[13]	4.6/5.4	13.5/11.5	1.02/0.8	>20	–	–
[15]	3.45/4.9	7.82/4.08	1.15/1.42	–	–	0.21×0.31

[16]	4.947	1.16	2.9	–	–	–
This work	3.61/5.55	12.5/10.81	0.4/1.7	21.5/28.3	19.8 (6.2–8)	0.25×0.30

Abbreviations: CF, central frequency; FBW, fractional bandwidth; IL, insertion loss; RL, return loss.

Performance comparisons of the presented dual-band BPF with filters designed in other previous works are listed in Table 2 showing that the proposed filter has good electrical performance in term of insertion and return losses, as well as compact size.

4. CONCLUSIONS

In this paper, open-loop SIRs with 50 Ω tapped input/output lines have been proposed to build dual-band BPF for licensed and unlicensed 5G bands in sub-6 GHz spectrum for mobile communications. Folding the two SIRs and choosing the appropriate value of the gap between the edges of the high-impedance lines help to create another transmission zero in the upper stopband. The proposed dual-band BPF is simulated and manufactured. The experimental results reveal 12.5% and 10.81% fractional bandwidths at 3.61 GHz and 5.55 GHz, respectively. The upper stopband extends more than 8 GHz with 19.8 dB rejection level. Compared with some reported works, this filter has merits of covering the licensed and unlicensed 5G bands, low insertion loss, good return loss and compact size with a low-cost methodology, making it suitable for 5G mobile communications.

ACKNOWLEDGEMENTS

The authors are grateful to the Department of Communication Engineering (DICOM), University of Cantabria (UNICAN), Spain, for support with regard to simulation software and facilities.

REFERENCES

[1] A. Osseiran et al., "Scenarios for 5G Mobile and Wireless Communications: The Vision of the METIS Project," IEEE Communications Magazine, vol. 52, no. 5, pp. 26–35, May 2014.

[2] X. Zhang, Y. Li, W. Wang and W. Shen, "Ultra-wideband 8-port MIMO Antenna Array for 5G Metal-frame Smartphones," IEEE Access, vol. 7, pp. 72273–72282, 2019.

[3] L. Liu, Q. Fu, F. Liang and S. Zhao, "Dual-band Filter Based on Air-filled SIW Cavity for 5G Application," Microwave and Optical Technology Letters, vol. 61, no. 11, pp. 2599–2606, Nov. 2019.

[4] D. Tharani, R. K. Barik, Q. S. Cheng, K. Selvajyothi and S. S. Karthikeyan, "Compact Dual-band SIW Filters Loaded with Double Ring D-shaped Resonators for Sub-6 GHz Applications," Journal of Electromagnetic Waves and Applications, vol. 35, no. 7, pp. 923–936, May 2021.

[5] W. Huang, L. Li, L. Li and J. Dong, "A Compact CPW Bandpass Filter Based on Spiral-shaped DGSs for 5G Frequency Band," Progress In Electromagnetics Research Letters, vol. 94, pp. 27–34, 2020.

[6] C. Karpuz, P. O. Ozdemir, H. Senol, A. Cengiz, H. H. Balik, and A. Gorur, "A Novel Concept in Design of Microwave Planar Dual Band Filter Having the Controllable Closed/Isolated Bands by Using the Simple Vias and the Slow Wave Effect for 5G/IoT Applications," Proc. of the 2021 IEEE 51st European Microwave Conf. (EuMC), London, United Kingdom, pp. 385–388, Apr. 2022.

[7] H. Zhang, K. Ma, W. Zhang and N. Yan, "A Novel Self-packaged DBBPF with Multiple TZs for 5G Sub-6 GHz Applications," Microwave and Optical Technology Letters, vol. 65, no. 1, pp. 62–68, 2023.

[8] Z. Xu, Y. Wu, Q. Dong and W. Wang, "Miniaturized Dual-band Filter Using Dual-mode Dielectric Waveguide Resonator," IEEE Microwave and Wireless Components Letters, vol. 32, no. 12, pp. 1411–1414, 2022.

[9] W.-L. Hsu, P.-Y. Lyu and S.-F. Chang, "Design of a Miniature Dual-band Bandpass Filter with Inter-locked Stepped-impedance Resonators for 5G New Radio Access Technology," Int. Journal of Microwave and Wireless Technologies, vol. 12, no. 8, pp. 733–737, Oct. 2020.

[10] A. Kapoor, P. Kumar and R. Mishra, "Analysis and Design of a Passive Spatial Filter for Sub-6 GHz 5G Communication Systems," Journal of Computational Electronics, vol. 20, no. 5, pp. 1900–1915, Oct. 2021.

[11] Y. Zhang, K. Ma and X. Chen, "A Compact Low-cost Dual-band Bandpass Filter with Enhanced Suppression Using Substrate Integrates Suspended Line Technology," Microwave and Optical Technology Letters, vol. 64, no. 2, pp. 276–282, 2022.

[12] D. Yang and Y. Dong, "Miniaturized Multilayer Surface-mountable 5G Filter Based on Shielded Spiral Resonator," IEEE Trans. on Circuits and Systems II: Express Briefs, vol. 69, no. 8, pp. 3366–3370, 2022.

[13] M. Riaz, B. S. Virdee, P. Shukla, K. Ouazzane, M. Onadim and S. Salekzamankhani, "Quasi-elliptic Dual-band Planar BPF with High-selectivity and High Inter-band Isolation for 5G Communications Systems,"

Microwave and Optical Technology Letters, vol. 62, no. 4, pp. 1509–1515, Apr. 2020.
[14] J.-S. Hong, Microstrip Filters for RF/Microwave Applications, 2nd Edn., DOI: 10.1002/0471221619, John Wiley & Sons, Inc., Hoboken, N.J: Wiley, 2011.
[15] W. Zhang, K. Ma, H. Zhang and H. Fu, "Design of a Compact SISL BPF with SEMCP for 5G Sub- 6 GHz Bands," IEEE Microwave and Wireless Components Letters, vol. 30, no. 12, pp. 1121–1124, Dec. 2020.
[16] N. Praveena and N. Gunavathi, "High Selectivity SIW Cavity Bandpass Filter Loaded CSRR with Perturbing *Vias* for Sub-6 GHz Applications," Progress In Electromagnetics Research Letters, vol. 109, pp. 103–110, 2023.

ملخص البحث:

تتناول هذه الورقة البحثية تصميم مرشِّح تمريرٍ مزدوج النّطاق لاستخدامه في الاتّصالات النّقّالة التي تنتمي الى الجيل الخامس. وقد تمّ استخدام أوّل تردُّدَي رنين للمِرْنان ذي الممانعة المتدرّجة في خطوات بوصفهما تردُّدَي التّشغيل لنطاقَي التّمرير للمرشِّح. علاوة على ذلك، تمّ طَيُّ المِرْنان ذي الممانعة المتدرّجة على خطوات لتشكيل مِرنان ذي حلقة مفتوحة وممانعة متدرّجة لأغراضٍ تتعلّق بالحصول على مرشِّح صغير الحجم لا يحتلّ حيّزاً كبيراً. وتتمّ تغذية المرشِّح عن طريق خطّ تغذية مقاومته 50 أوم.

تمّت تجربة المرشِّح عملياً، وأُجريت له محاكاةٌ بواسطة الحاسوب، حيث اتّضح وجودُ اتّفاقٍ جيّد بين نتائج التّجربة ونتائج المحاكاة. وتبين من التّحليل أنّ فقْد الإرجاع للمرشِّح بلغ 21.5 ديسيبل، و 28.3 ديسيبل، بينما بلغ فقْد الإدخال 0.4 ديسيبل و 1.7 ديسيبل، و أمّا عرض النّطاق للمرشِّح فبلغ 12.5% و 10.81%، وذلك عند التّردُّدَين 3.61 جيجاهيرتز و 5.53 جيجاهيرتز على الترتيب.

كذلك جرت مقارنة أداء المرشِّح المقترح بأداءات عددٍ من المرشِّحات الواردة في الدّراسات السابقة، حيث اتّضح أنّ المرشِّح الذي تم تصميمه وتحليله في هذا البحث حقّق نتائج مُرْضِية. فبالإضافة الى النّتائج المذكورة من حيث فقْد الإرجاع وفقْد الإدخال والنّطاق التردُّدي، تميّز المرشِّح المقترح بصغر الحجم، مما يجعله ملائماً للاستخدام في اتّصالات الجيل الخامس النّقّالة لنطاقات تردُّدية فرْعية ضمن التّردُدات حتى 6 جيجاهيرتز.